A Microphysical Retrieval Scheme for Continental Low-Level Stratiform Clouds: Impacts of the Subadiabatic Character on Microphysical Properties and Radiation Budgets

HUNG-NENG S. CHIN, DANIEL J. RODRIGUEZ, RICHARD T. CEDERWALL, CATHERINE C. CHUANG, ALLEN S. GROSSMAN, AND JOHN J. YIO

Atmospheric Science Division, Lawrence Livermore National Laboratory, Livermore, California

QIANG FU

Atmospheric Sciences Program, Dalhousie University, Halifax, Nova Scotia, Canada

MARK A. MILLER

Division of Applied Science, Brookhaven National Laboratory, Upton, New York

(Manuscript received 16 February 1999, in final form 8 September 1999)

ABSTRACT

Using measurements from the Department of Energy's Atmospheric Radiation Measurement Program, a modified ground-based remote sensing technique is developed and evaluated to study the impacts of the subadiabatic character of continental low-level stratiform clouds on microphysical properties and radiation budgets. Airborne measurements and millimeter-wavelength cloud radar data are used to validate retrieved microphysical properties of three stratus cloud systems occurring in the April 1994 and 1997 intensive observation periods at the Southern Great Plains site.

The addition of the observed cloud-top height into the Han and Westwater retrieval scheme eliminates the need to invoke the adiabatic assumption. Thus, the retrieved liquid water content (LWC) profile is represented as the product of an adiabatic LWC profile and a weighting function. Based on in situ measurements, two types of weighting functions are considered in this study: one is associated with a subadiabatic condition involving cloud-top entrainment mixing alone (type I) and the other accounts for both cloud-top entrainment mixing and drizzle effects (type II). The adiabatic cloud depth ratio (ACDR), defined as the ratio of the actual cloud depth to the one derived from the adiabatic assumption, is found to be a useful parameter for classifying the subadiabatic character of low-level stratiform clouds. The type I weighting function only exists in the lower ACDR regime, while the type II profile can appear for any adiabatic cloud depth ratio.

Results indicate that the subadiabatic character of low-level stratiform clouds has substantial impacts on radiative energy budgets, especially those in the shortwave, via the retrieved LWC distribution and its related effective radius profile of liquid water. Results also show that this subadiabatic character can act to stabilize the cloud deck by reducing the in-cloud radiative heating/cooling contrast. As a whole, these impacts strengthen as the subadiabatic character of low-level stratiform clouds increases.

1. Introduction

The significance of low-level stratiform clouds to the planetary radiation balance is due to their persistence and coverage, and their effect on the planetary albedo. On the annual average, their fractional coverage is about 25% of the globe (Hartmann et al. 1992). It has been estimated that a change of low-level cloud cover, or cloud albedo, by only a few percent could offset or double the greenhouse warming (Ramanathan et al. 1989). Therefore, accurate representation of these clouds in global climate models (GCMs) is critically important.

To this end, the Department of Energy's (DOE's) Atmospheric Radiation Measurement (ARM) program employs specialized surface-based remote sensors to improve the parameterization of these clouds. Such measurements are performed at several locations around the world, including the Southern Great Plains (SGP) area of the United States. Using data from a combination of surface-based sensors, it is possible to develop microphysical retrieval algorithms that provide information

Corresponding author address: Dr. Hung-Neng S. Chin, Lawrence Livermore National Laboratory, P.O. Box 808 (L-103), Livermore, CA 94551.
E-mail: chin2@llnl.gov

about particle size and number density in clouds composed of either ice or liquid.

In many microphysical retrieval algorithms, information about the detailed internal microphysical structure of clouds is determined by relating the profile of millimeter-wavelength cloud radar (MMCR) reflectivity to some aspect of the cloud particle spectrum. However, such a relationship has not yet been resolved for low-level liquid clouds. Therefore, the radar reflectivity profile of liquid clouds must be related to the retrieved liquid water content (LWC) with additional assumptions, such as the shape of the droplet spectrum (Frisch et al. 1995), the adiabatic condition, and no hydrometeor fallout (Liao and Sassen 1994; Paluch et al. 1996).

Furthermore, routine application of the most sophisticated microphysical retrieval schemes can be impeded by the contamination of microwave radar reflectivities by echoes from insect and biological debris entrained into low-level stratiform clouds as occurs at the ARM SGP site during the warm season. Consequently, it is of value to use algorithms that do not require a radar reflectivity profile as the principal measurement to obtain usable information.

There exist cloud retrieval algorithms that do not rely on radar reflectivity profiles (e.g., Han and Westwater 1995, hereafter referred to as the HW scheme; Dong et al. 1997). These algorithms are designed to estimate microphysical properties at locations where microwave radar measurements are unavailable, and rely on data from active and passive sensors and radiative transfer models as constraints. Inevitably, this type of algorithm contains more assumptions since active measurements of the internal cloud properties are not usually obtainable. Furthermore, solar irradiance data are required in Dong's algorithm, so this technique can only be applied during the daytime.

In the HW scheme, the retrieved LWC profile is derived based on the adiabatic assumption. On occasion, this scheme works quite well for some stratus and stratocumulus clouds, which are nearly adiabatic (Albrecht et al. 1990). However, many in situ measurements of these clouds show that the adiabatic LWC ratio, defined as the ratio of LWC to its adiabatic value, decreases with height from the cloud base to the cloud top (Albrecht et al. 1985; Nicholls and Leighton 1986; Rogers and Telford 1986; Ishizaka et al. 1995). In extreme cases, this ratio can be as low as 0.1–0.2 near the cloud top. Many earlier studies have documented the cause of the subadiabatic character of low-level clouds as being the result of vertical and/or lateral mixing processes, and the drizzle effect (Cotton 1975; Deardorff 1980; Albrecht et al. 1985; Chen and Cotton 1987).

Airborne measurements of stratus and stratocumulus clouds over oceans and islands indicate that vertical distributions of the adiabatic LWC ratio profiles generally fall into two distinct categories (Fig. 1). One set, referred to as type I, is nearly adiabatic near the cloud base, but begins to drop off rapidly near the cloud top,

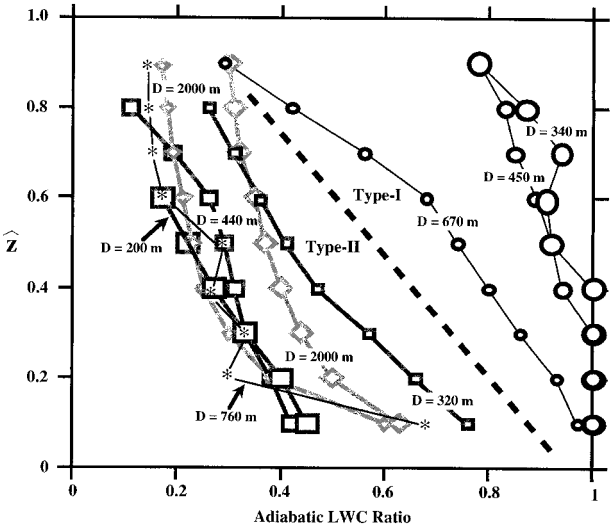

FIG. 1. Ratios of observed liquid water content profiles from airborne measurements to their adiabatic values. The vertical coordinate is the scaled height between the cloud base and cloud top. The lines connecting circles indicate samples of marine stratus (adapted from Nicholls and Leighton 1986); squares, marine stratocumulus (Albrecht et al. 1985); asterisk, stratus over an island (Ishizaka et al. 1995); and diamonds, small cumulus (Cotton 1975). The D in each profile stands for the cloud depth. The thick dashed line separates the regimes for type I and type II adiabatic LWC ratio profiles.

while the other one, labeled type II, varies in an opposite sense. Both types of adiabatic LWC ratio profiles can exhibit substantial subadiabatic character. The vertical variations of type I adiabatic LWC ratio profiles agree well with the anticipated impact of cloud-top entrainment mixing. The general character of type II adiabatic LWC ratio profiles is similar to that of small cumulus, in which both cloud-top and lateral entrainment mixing processes are important mechanisms leading to the depletion of liquid water. However, it is generally believed that lateral entrainment is less important in the low-level stratiform clouds. It would, therefore, be interesting to know in this study whether the drizzle effect is the main factor to cause the difference of these two types of adiabatic LWC ratio profiles.

The subadiabatic character of low-level stratiform clouds was also reported in midlatitude continental cases (Politovich et al. 1995). This study showed that low-level clouds with strong subadiabatic character (ratio of the integrated LWC to its adiabatic value is less than 50%) account for about 65% of the cloud population. In addition, approximately 50% of these clouds had an adiabatic cloud depth ratio (ACDR), defined as the ratio of the actual cloud depth to the one derived from the adiabatic assumption, greater than two. Therefore, the use of the adiabatic assumption in the retrieval techniques can lead to a noticeable underestimation of the cloud depth and an overestimation of the maximum LWC for a significant portion of low-level clouds. As a result, the inappropriate retrievals of cloud micro-

physical properties may have substantial impacts on the in-cloud heating profile and radiative transfer due to the strong cloud–radiation interaction.

In this paper, we demonstrate a cloud retrieval technique without using microwave radar measurements as the requirement to retrieve the internal cloud structure. This technique is developed by modifying the HW scheme to provide a more realistic portrayal of the retrieved liquid water for low-level liquid clouds with substantial adiabatic character. This new retrieval technique is evaluated using measurements from the DOE's ARM program at the SGP site. The applicability of this new algorithm depends on the availability of the cloud-top heights. There are, of course, situations when cloud-top height information may be unavailable from a microwave radar because of echo contamination. Therefore, cloud-top height information from other sources, such as lidars, wind profilers, and radiosondes, enables this retrieval algorithm to be used in a variety of circumstances. However, this information should be determined with caution due to the inherent limitation of each instrument.

The main objective of this study is to assess the impacts of the subadiabatic character of low-level stratiform clouds on cloud microphysical properties and radiation budgets by examining the sensitivity of the retrieved cloud structure to cloud optical properties and radiative transfer. The modified HW retrieval algorithm acts as a diagnostic tool to this end. Another objective is to evaluate the feasibility of using radiosonde and ground-based remote sensor data to retrieve microphysical properties of low-level stratiform clouds at the boundary facilities of the SGP site, where MMCR data are unavailable.

The paper is organized as follows. Section 2 describes the instruments and observations used to develop and to validate the modified HW retrieval scheme. The details of this retrieval scheme, which eliminates the need to use the adiabatic assumption in the retrieved LWC profiles, is presented in section 3. Section 4 shows comparisons of retrieved microphysical properties with observations, and their impacts on cloud optical properties and radiation budgets. A summary and discussion follow in section 5. For simplicity in describing the figures with the vertical profiles of any physical variables, the vertical axis shown in heights is referred to the mean sea level unless otherwise mentioned.

2. Instruments and observations

a. Instruments

In this study, the HW scheme is used as a ground-based tool to retrieve the cloud microphysical properties of low-level stratiform clouds at the central facility (C1) of ARM's SGP site. Along with the use of the adiabatic assumption (i.e., no mixing and no fallout of condensed moisture), the HW scheme adopts data from a suite of ground-based sensors to determine the cloud-top height, and profiles of water vapor and LWC. These instruments provide the following inputs to the HW scheme: 1) two microwave brightness temperatures from a dual-channel microwave radiometer, one at a vapor sensitive frequency of 23.8 GHz and the other at a water sensitive frequency of 31.4 GHz; 2) virtual temperature from a radio acoustic sounding system; 3) cloud-base height from a laser ceilometer; and 4) surface temperature, pressure, and humidity from conventional surface meteorological instruments.

Note that the virtual temperature in this study is given from the radiosonde data, which have greater vertical extent and resolution than the data retrieved from a radio acoustic sounding system. The noise level of retrieved the liquid water path (LWP) of the microwave radiometer is 0.003 mm. However, any statistical retrieval is essentially a multiple linear regression, which is involved in a residual error. In this LWP retrieval, the residual error or theoretical accuracy of the instrument is 10 times the noise level. An LWP of 0.03 mm retrieved from a microwave radiometer could be clear sky. Any LWP above this threshold value is considered as a detectable quantity for the cloudy condition. When the retrieved LWP exceeds 1 cm, this reading is treated as an invalid report. Such a large value of LWP is not physically possible, and it indicates a serious failure of the retrieval, most likely due to drizzle or rainfall standing on the instrument.

The products retrieved by the HW scheme, such as water vapor density profile, LWC profile, integrated water, vapor and LWC, are obtained through an iteration process, which involves both statistical and physical retrievals (see the upper part of Fig. 2). In this study, the statistical retrieval is based on an ensemble of 17 218 radiosonde soundings from Oklahoma City, Tinker AFB, and Norman, Oklahoma, during the springtime of 1966–92. These sounding stations are located about 110~130 km to the south of the central facility of the SGP site. The readers are referred to Han and Westwater (1995) for further details of the instruments and the retrieval algorithm.

With a modification resulting from the addition of cloud-top height information into the retrieval algorithm (see the lower part of Fig. 2), the original applications of the HW scheme can be expanded to include low-level clouds having substantial subadiabatic character as is often observed in stratus and stratocumulus clouds.

Instruments aboard the Pacific Northwest National Laboratory's Gulfstream and the University of North Dakota's Citation aircrafts provided data on the in situ microphysical properties of low-level stratiform clouds near the central facility of the SGP site for validation purposes. These measurements include 1) LWC from a King probe and a forward scattering spectrometer probe (FSSP) on the Citation, 2) LWC from a King probe and a particle volume monitor system (PVM) on the Gulfstream, and 3) mean volume radii of cloud droplets (r_v)

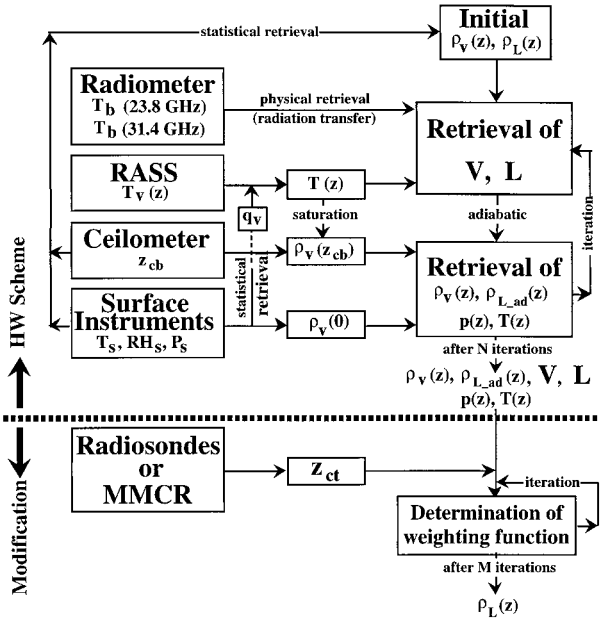

FIG. 2. A schematic diagram of the system used to retrieve profiles of temperature $T(z)$, water vapor $\rho_v(z)$, cloud liquid water $\rho_L(z)$, adiabatic cloud liquid water $\rho_{L\_ad}(z)$, integrated water vapor V, and integrated cloud water L from measurements of microwave brightness temperatures T_b at 23.8 and 31.4 GHz, virtual temperature profile $T_v(z)$, cloud-base height z_{cb}, cloud-top height z_{ct}, surface temperature T_s, relative humidity RH_s, and pressure P_s; $\rho_v(0)$ and $\rho_v(z_{cb})$ are water vapor density at the surface and cloud-base height, respectively. The flow chart above the dashed line is adapted from Han and Westwater (1995). Extension of the HW scheme is accomplished with the addition of a new methodology shown in section 3.

and droplet number concentrations (N) from the FSSP probe on the Citation. Radar reflectivity data from ARM's millimeter-wavelength cloud radar are also used to help validate the retrieved in-cloud microphysical properties.

b. Observations

Three stratus cloud systems, observed at the central facility of ARM's SGP site on 30 April 1994 (referred to as case A), 9 April 1997 (case B), and 12 April 1997 (case C) are considered in this study. These cloud systems developed under different boundary layer conditions. Cases A and C occurred in a well-mixed boundary layer, with case A being in a warmer, moister environment than case C. Case B was associated with a decoupled boundary layer, accompanied by a low-level surge of cold, dry air outbreak starting at 0200 UTC 9 April 1997 or so (elaborated upon shortly).

In situ measurements from the Citation aircraft were available to validate cases A and B, and the Gulfstream aircraft provided airborne data for case C. Also, the millimeter-wavelength cloud radar was operating during cases B and C (see Table 1). The cloud system on 9 April 1997 (case B) was sampled by the Citation aircraft only during its dissipation stage, but the substantial subadiabatic character of this stratus cloud appeared earlier. Therefore, the retrieved cloud properties in cases A and C can be verified using in situ measurements, while these properties in case B can only be validated using millimeter-wavelength cloud radar data.

TABLE 1. Lists of available airborne and millimeter-wavelength cloud radar measurements. Information in parentheses identifies the date and the aircraft used in the collection of data for each case. Superscript asterisks indicate a mismatch between in situ measurement and the analysis periods for case B, and plus signs for the poor data quality of case C. Other notations are described in the text.

	Case A (Citation) (30 Apr 1994)	Case B (Citation) (9 Apr 1997)	Case C (Gulfstream) (12 Apr 1997)
King	LWC	*LWC	$^{+}$LWC, $^{+}r_e$, ^{+}N
FSSP	LWC, r_v, N	*LWC, $*r_v$, $*N$	—
PVM	—	—	LWC, $^{+}r_e$
MMCR	—	dBZ	dBZ

Airborne measurements of case A from the Citation were available every second. To mitigate the impact of multiple penetrations of different cloud tops in a spiral-up flight path, 10-s running-averaged data are used to alleviate horizontal variation of airborne measurements and to compare with the retrieved microphysical properties (Fig. 3).

The in situ data of case C from the Gulfstream were also available every second. However, the King LWC probe worked improperly and other microphysical properties, such as the effective size of cloud droplets (r_e) and the droplet number concentration (N), were either questionable or unavailable. As a result, the only microphysical property that could be used for validation was the PVM-measured LWC. This LWC profile (Fig. 4a) exhibits a complicated seesaw pattern near the cloud tops during an ascending flight path. Unlike the Citation's spiral-up flight path in case A, the Gulfstream went through a series of ascents and descents between

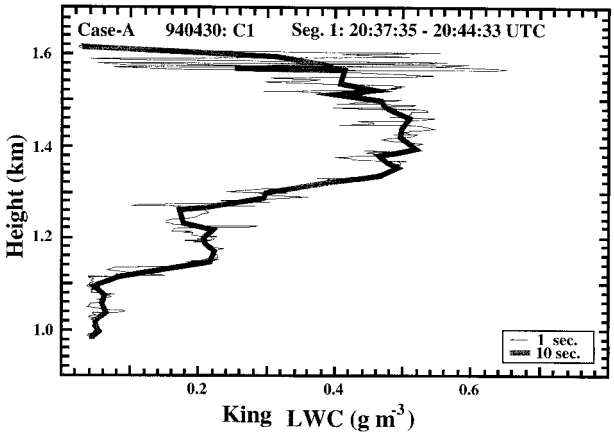

FIG. 3. Vertical profiles of LWC measured by a King probe in a stratus cloud near the central facility of the SGP site on 30 Apr 1994 during a flight by the University of North Dakota Citation aircraft. Times are indicated by h:min:s.

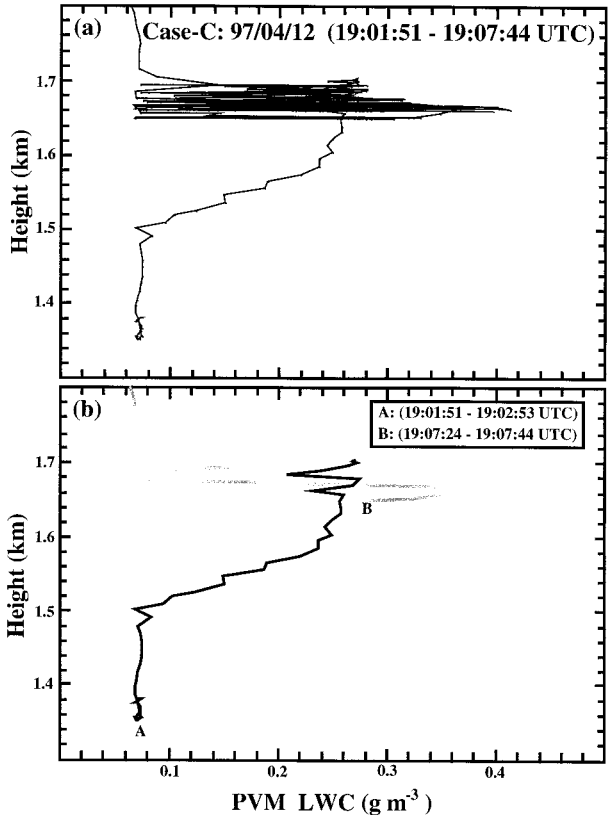

FIG. 4. As in Fig. 3 except for the stratus cloud in case C occurring on 12 Apr 1997 during a flight by the Pacific Northwest National Laboratory's Gulfstream aircraft.

1.65 and 1.70 km to sample aerosols so as to satisfy another aspect of the flight mission. Combined with rapid changes in cloud-top heights (shown in section 4a), the use of a temporal average of the measured LWC data would provide a misleading picture in the vertical structure of composite LWC profile. Therefore, only subsets of the 1-s data at the very beginning and end of this flight path (Fig. 4b) are used for comparison against the retrieved LWC profiles. Millimeter-wavelength cloud radar data are also used to help validate this case.

As far as the modified retrieval algorithm is concerned, the cloud-top information can be obtained from any instrument. To demonstrate the capability of this modified retrieval algorithm in providing microphysical properties without using microwave radars, the cloud-top height estimated from the radiosonde measurements is used in this study. As in the HW scheme, the cloud base information required to run the retrieval algorithm is given from the ceilometer, instead of being given from the sounding profile as a result of the sensor saturation problem near the cloud base.

Radiosonde data (such as temperature, dewpoint temperature, horizontal winds) available every 3 h, and surface observations and ground-based remote sensor measurements at 5-min intervals, were used to retrieve the microphysical and optical properties of stratiform clouds. In addition, millimeter-wavelength cloud radar data were obtained from four operational modes over 36 s. Clothiaux et al. (1999) indicated that this temporal resolution provides an accurate depiction of clouds in a vertical column above the radar. As seen in the millimeter-wavelength cloud radar, all three of these cloud systems were single-layer stratus clouds, located beneath an inversion layer aloft (Figs. 5a, 6a, and 7a). Although the inversion layer in case C is less evident than the ones in the other two cases, substantial vertical gradients of temperature and/or moisture near the cloud top enable us to use radiosonde data for determining the cloud top.

The thermodynamical structure in case B reveals a decoupling of cloud and subcloud layers (Fig. 6b),

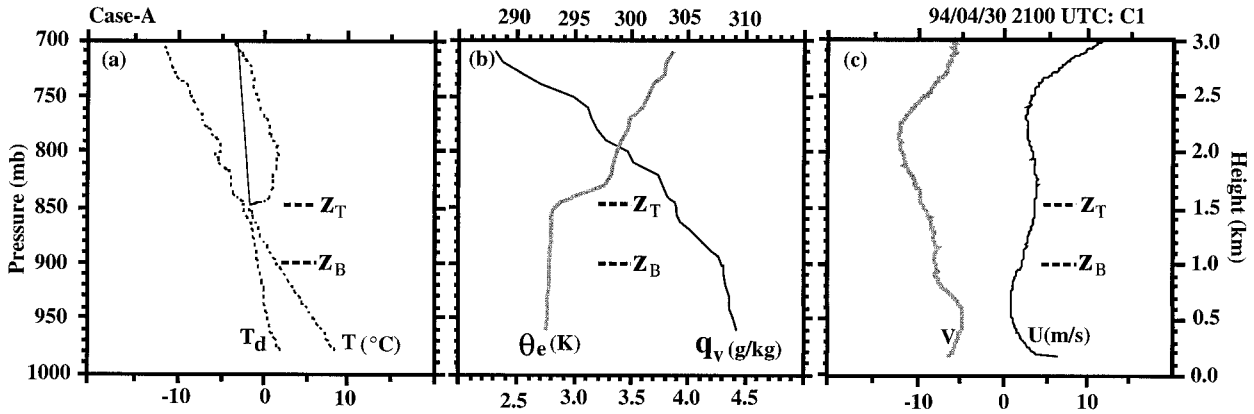

FIG. 5. Vertical profiles of radiosonde-measured data for case A at C1 of the ARM SGP site at 2100 UTC 30 Apr 1994: (a) temperature and dewpoint temperature, (b) equivalent potential temperature (θ_e) and water vapor mixing ratio (q_v), and (c) zonal and meridional components of the horizontal velocities. Thick dashed lines mark the cloud-top (Z_T) and cloud-base heights (Z_B), determined by the soundings and the ceilometer, respectively. The modified temperature profile, marked by the solid line above the temperature inversion layer in (a), is used for a sensitivity experiment described in Fig. 17b.

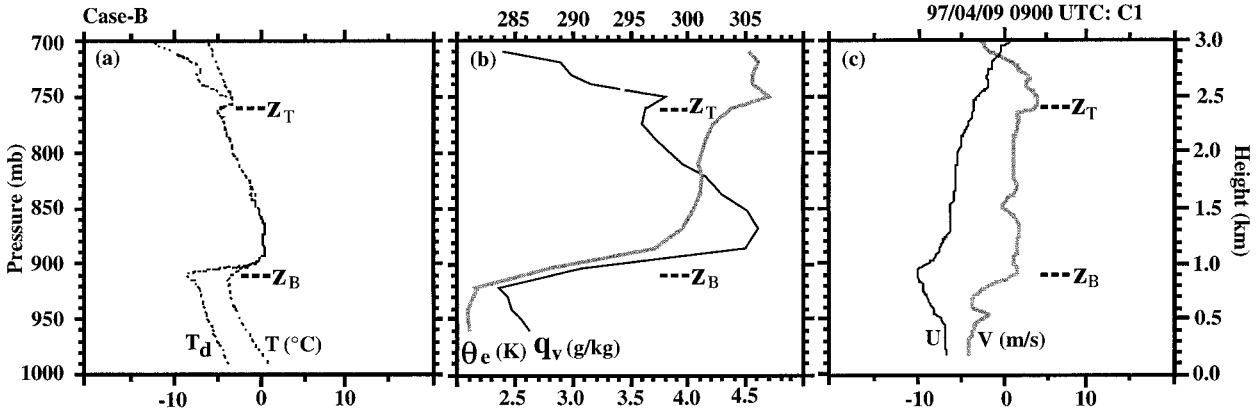

FIG. 6. As in Fig. 5 except for case B at 0900 UTC 9 Apr 1997.

which differs significantly from their counterparts in cases A and C (Figs. 5b and 7b) as a result of a cold, dry air intrusion of a high pressure system from Canada (Fig. 8). Therefore, the cold air beneath the cloud base and the subsidence warming above the cloud top in case B cause a sharp discontinuity in the equivalent potential temperature (θ_e profile near the cloud top and cloud bottom (Fig. 6b). Due to sufficient wind shear near the cloud boundaries, these sharp discontinuities are, to some extent, weakened by the mixing process (Fig. 6c). This cooling/heating contrast can also act to stabilize the cloud layer. In contrast, the θ_e profiles in cases A and C remain nearly constant in coupled cloud and subcloud layers.

3. Modified retrieval scheme

As shown in Fig. 1, profiles of measured LWCs in both marine and continental low-level stratiform clouds often exhibit substantial subadiabatic character. Therefore, a methodology that extends the applicability of the HW scheme for retrieving the microphysical properties of low-level clouds is proposed in this study. The addition of cloud-top height information into the HW scheme eliminates the need to invoke the adiabatic assumption, while two other constraints of the HW scheme (i.e., a single-layer cloud and the cloud temperature warmer than -20°C) remain in effect. This limitation is, however, fairly justified for the low-level stratiform clouds considered.

In this modified cloud retrieval scheme, the LWC profile is represented by the product of an adiabatic LWC profile and a weighting function. This weighting function, also called the adiabatic LWC ratio (ALWCR) profile, is defined as the ratio of the retrieved LWC profile to its adiabatic value. The adiabatic LWC profile is determined from the HW scheme once the cloud-base height from a ceilometer and the integrated LWC from a microwave radiometer are provided. As seen in the observations, there exist two distinct types of weighting functions (Fig. 1). Both types of weighting functions can be expressed in the same form, given by $f(\hat{z}) = \exp(-\alpha \cdot \hat{z}^{\beta})$, where $\hat{z}$ is the scaled height within the cloud deck, and α and β are two positive constants representing the departure of LWC from its adiabatic value and the curvature of the weighting function, respectively. As discussed earlier, we postulate that the type I adiabatic LWC ratio profile only accounts for

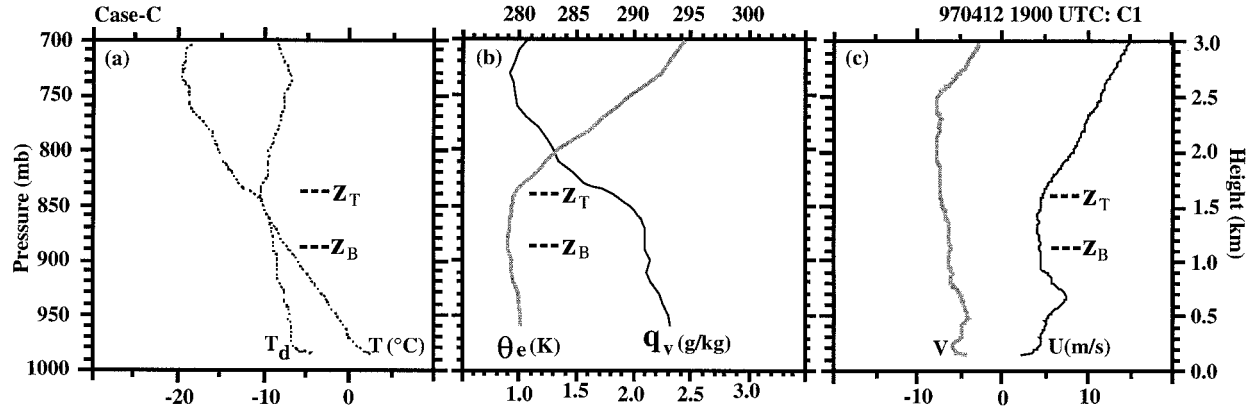

FIG. 7. As in Fig. 5 except for case C at 1900 UTC 12 Apr 1997.

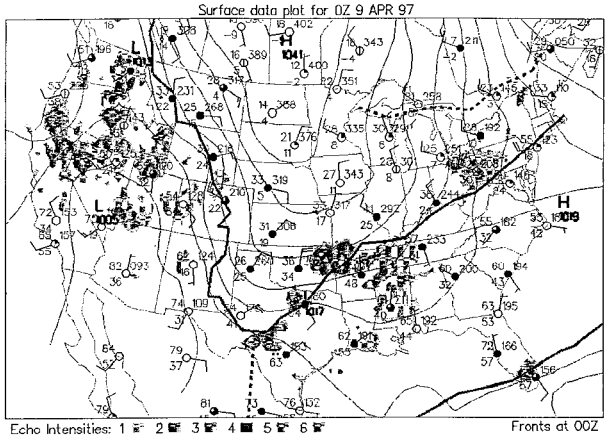

FIG. 8. The presynoptic condition of case B stratus cloud. Surface weather map at 0000 UTC 9 Apr 1997.

cloud-top entrainment mixing, while the type II profile considers both mixing and drizzle effects.

Figure 9 shows the sensitivity of the vertical variation of the weighting function to parameters α and β. As shown in this figure, the general character of adiabatic LWC ratio profiles is primarily determined by the parameter β. A value of $\beta > 1$ represents a type I weighting function, while $\beta < 1$ corresponds to a type II adiabatic LWC ratio profile. Results also indicate under the given parameter α the change of each type of weighting functions due to the varied parameter β is not trivially small although this change is much smaller than its counterpart with the varied α under the given β. However, the parameter β is interrelated to α in determining the weighting function for the given LWP and cloud depth in this retrieval algorithm. As a result, any type of weighting functions with a larger β would have a larger α to keep LWP the same in the cloud deck. Due to the self-adjustment feature of this retrieval algorithm, the weighting functions of each type with different β values would be very close to each other, and their difference exists mainly in the lower half of the cloud deck, where the adiabatic LWC is small. Therefore, the difference between retrieved LWC profiles with varied β values is fairly small. Using the data from case A, the impact of this change on the retrieved LWC profiles is 4.8% and 6.2% for the maximum values of type I ($\beta = 2$ and 4) and type II ($\beta = 0.25$ and 0.5), respectively. As a result, the parameter β is treated as an insensitive parameter to the retrieved LWC profiles, and set as a constant ($\beta = 4$ for type I and $\beta = 0.5$ for type II) to represent the general character of the weighting function in this study.

Referring to Fig. 1, there might exist a mixed type of observed adiabatic LWC ratio profiles in the right portion of Fig. 1 (e.g., the one labeled D = 340 m),

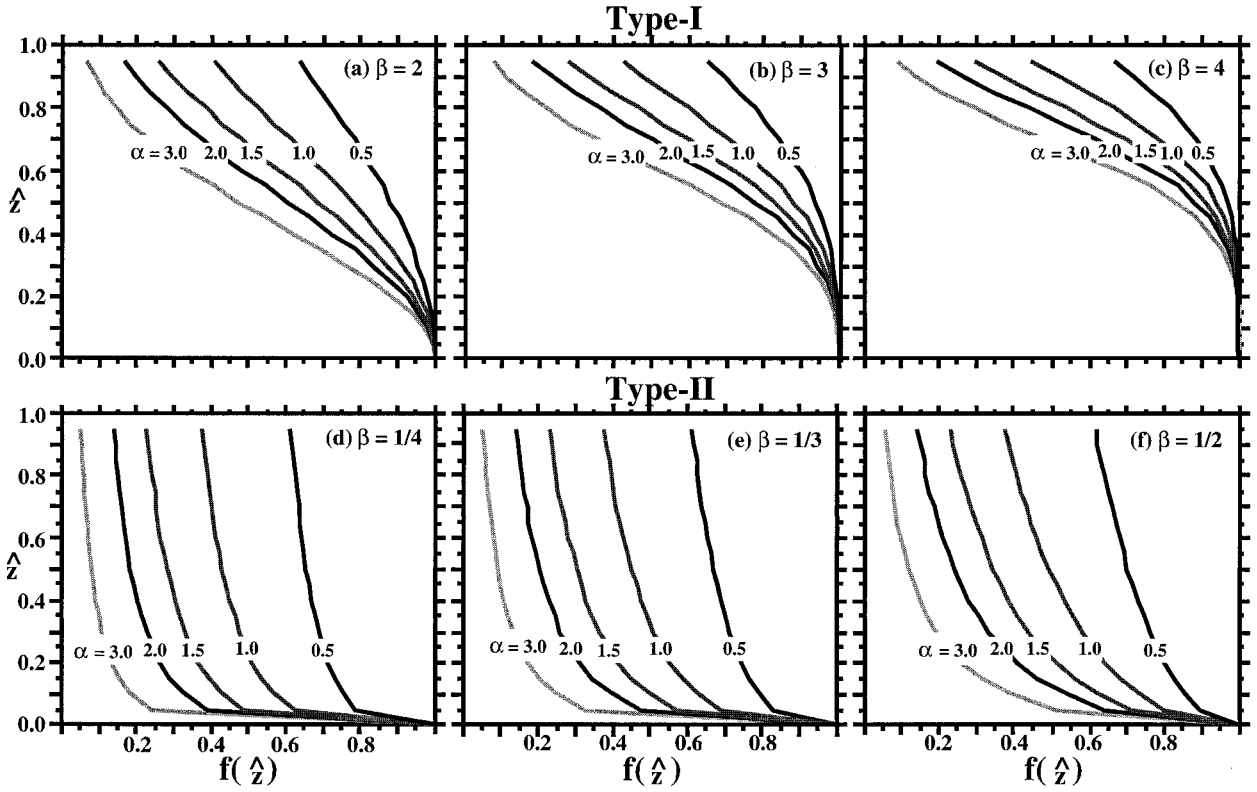

FIG. 9. Vertical profiles of the weighting functions for varied parameters α and β: (a)–(c) $\beta > 1$ for the type I weighting function, (d)–(f) $\beta < 1$ for the type II weighting function.

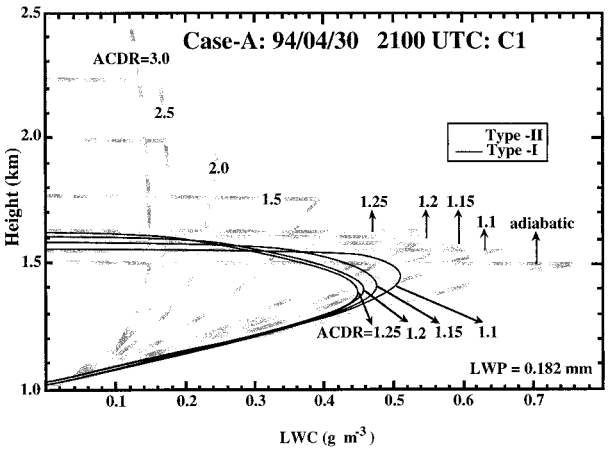

FIG. 10. Vertical profiles of retrieved LWCs based on radiosonde and remote sensor data from case A at 2100 UTC 30 Apr 1994 at the central facility of the SGP site, and specified cloud-top heights (represented by different adiabatic cloud depth ratios) under the given liquid water path (LWP).

where type I and type II variations appear in the upper and lower parts of the mixed type weighting function, respectively. It is not certain whether the subtle variation in the lower part of this mixed type weighting function is due to the uncertainty of in situ measurements. To gauge this impact, a sensitivity test with the mixed type weighting function (i.e., type I in the upper portion and type II in the lower part) was conducted and compared with the results using type I and type II weighting functions, respectively. Results (not shown) indicate that the retrieved LWC profile using the mixed type weighting function is very close to the one using the type I adiabatic LWC ratio profile. This result is not surprising because most of the LWC in low-level clouds appears in the upper part of the cloud deck. Therefore, this study only uses two types of weighting functions to characterize the subadiabatic character of the retrieved LWC profiles.

Based on in situ measurements as shown in Fig. 1, the adiabatic LWC ratio is assumed to be zero at the cloud top and unity at the cloud base. The weighting function for each type of adiabatic LWC ratio profile is thus uniquely known via an iteration process (see the lower part of Fig. 2). This iteration process determines the corresponding parameter α under the given cloud geometry (i.e., cloud-base and cloud-top heights) and integrated LWC. The tolerance of the cloud-top height difference between retrieved and observed ones is set to 5 m in the iteration process.

Using the data from case A and different prescribed cloud-top heights, the general solutions of this cloud retrieval algorithm for the given LWP and the cloud-base height are summarized in Fig. 10. This figure clearly indicates that both types of LWC profiles can exist in the low adiabatic cloud depth ratio regime (i.e., ACDR $\leq$ 1.25). The vertical structures of both types of retrieved LWCs are very different; each type II profile exhibits a monotonic increase of LWC with height above the cloud base, followed by a rapid dropoff near the cloud top, while the type I profile is a skewed-parabolic distribution of LWCs within the cloud deck. The patterns of these retrieved LWC profiles in the low adiabatic cloud depth ratio regime were also observed in marine stratiform clouds (Slingo et al. 1982) since the majority of these clouds appear to have small ACDRs or weak subadiabatic character. Another interesting feature of this figure is that the altitudes of maximum LWC of type I and type II profiles separate farther as the adiabatic cloud depth ratio increases.

When the adiabatic cloud depth ratio exceeds a threshold value of 1.25, the iteration process cannot converge for the type I weighting function since the difference of retrieved and observed cloud-top heights cannot fall into the specified tolerance level. Therefore, only the type II adiabatic LWC ratio profiles can exist and their vertical distribution changes noticeably. For the case with a very large adiabatic cloud depth ratio (say, ACDR $\geq$ 2.5 where the adiabatic LWC ratio is about 0.1 near the cloud top), the retrieved type II LWC profile tends to be more uniform throughout the cloud deck. This type of LWC profile is an indication of having substantial subadiabatic character throughout the cloud deck, and has been observed in a marine stratiform cloud sheet (Nicholls and Leighton 1986). For an adiabatic cloud depth ratio of 3.0, the retrieved adiabatic LWC ratio near the cloud top is as low as 0.058, which is rarely observed in the low-level stratiform clouds. Therefore, this large adiabatic cloud depth ratio value might be viewed as the upper limit of low-level stratiform clouds. The overall features of Fig. 10 also appear in the cases with different LWPs (e.g., cases B and C; not shown) observed in other ARM April intensive observation periods (IOPs).

As a whole, both type I and type II LWC profiles are the possible solutions of the retrieved cloud structure when the LWP is only slightly less than its adiabatic value (i.e., high adiabatic LWP ratio case). In other words, this cloud retrieval algorithm appears to be ill-posed in the low adiabatic cloud depth ratio regime. Therefore, there is no unique solution in this circumstance unless additional information, such as the presence of drizzle, is available. This information can be given from airborne measurements or millimeter-wavelength cloud radar. When the LWP is much less than its adiabatic value (i.e., low adiabatic LWP ratio case), the iteration process does not converge for the type I profile, so the type II profile is the only solution.

Between the two extremes outlined above, the choice of weighting functions is arbitrary and can be made on the basis of the adiabatic cloud depth ratio or the adiabatic LWP ratio; both are measures of the degree to which the liquid water content is less than that predicted on the basis of the adiabatic assumption. Regardless of which measure is used, the threshold value is a critical

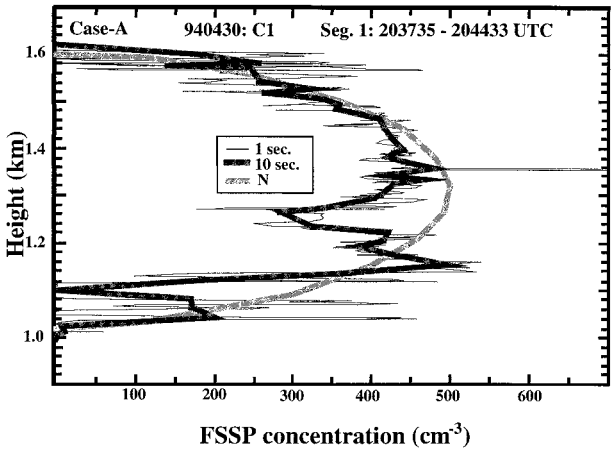

FIG. 11. As in Fig. 3 except for the droplet number concentrations measured by the FSSP during case A. Here, N is the approximated profile used for retrieving the effective radius of droplets in this study.

parameter that causes the algorithm to switch the retrieved solutions from the multiple modes of solutions to the single mode regime. Based on sensitivity tests using ARM data from several April IOPs, this threshold value is found to be 0.6 for the adiabatic LWP ratio and 1.25 for the adiabatic cloud depth ratio.

Along with the droplet number concentration (N) from the observations, the information shown in Fig. 10 can also be used to gauge the impact of retrieved cloud microphysical properties on radiation budgets (elaborated upon in section 4b). To determine the optical properties of low-level stratiform clouds, it is necessary to know the effective radius of cloud droplets (r_e). Following Martin and Johnson (1992), we use $r_e = 1.15 \cdot r_v$ in this study; the factor of 1.15 is based on observations of the continental air mass from the First ISCCP (International Satellite Cloud Climatology Project) Regional Experiment; FATE First ATSR (Along Track Scanning Radiometer) Tropical Experiment, and around the United Kingdom. The mean volume radius of cloud droplets (r_v) is given by

$$\left(\frac{0.75\text{LWC}}{\pi N \rho_w}\right)^{1/3},$$

where ρ_w is the liquid water density.

Due to the great variation of observed N between ocean and continent, and impacts from anthropogenic pollution (e.g., Twomey et al. 1984; Leaitch et al. 1992), it remains a research effort to parameterize N. Therefore, an approximated profile of N to the observed is used in this study to derive the r_e profile under the given retrieved LWC, and to examine the sensitivity of different weighting functions to the retrieved microphysical and optical properties of low-level stratiform clouds. This droplet number concentration profile is formulated by $N_0 \cdot [\sin(\tau \cdot \hat{z})]^{1/2}$, where N_0 is given by the maximum value of the observed N profile and $\hat{z}$ the normalized

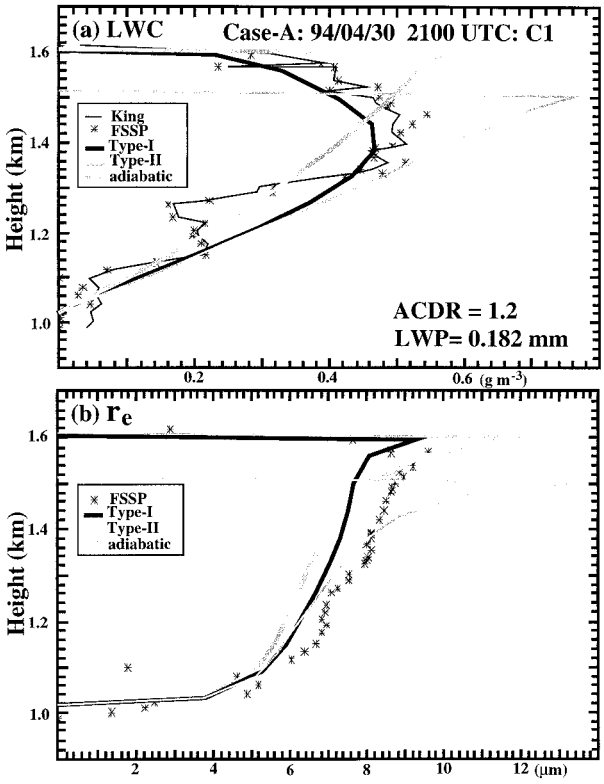

FIG. 12. Vertical profiles of retrieved and in situ measured microphysical properties for case A: (a) LWC, and (b) effective radius (r_e) of liquid water.

scale height within the cloud deck. The square root of the distribution accounts for the rapid decrease of N near the cloud boundaries and nearly constant N within the remainder of the cloud deck. Figure 11 exhibits both the observed and approximated N profiles of case A. Although the observed profile shows more small-scale fluctuations, the approximated N profile is frequently seen in marine stratus and stratocumulus clouds (Slingo et al. 1982; Nicholls 1984; Noonkester 1984; Martin et al. 1994; Albrecht et al. 1995). Similar to the retrieved LWC profile, the observed r_e profile of case A does not exhibit an evident change near 1.25 km (see Figs. 11 and 12); this might arise from the offsetting effect of observed LWC and N on r_e.

In addition to the radiation transfer model required for the determination of integrated water vapor and LWC in the HW scheme (Westwater 1978), another radiation model (Fu and Liou 1993; Fu et al. 1997) is used to diagnose cloud optical properties, and to compute longwave (LW) and shortwave (SW) radiation fluxes and heating/cooling rates. These radiation calculations assume the plane-parallel cloudy atmosphere. This assumption was recently assessed by Fu et al. (2000), using a three-dimensional (3D) broadband solar radiation model to examine the cloud geometry effect. Their results showed that the cloud 3D structure has little effects on the atmospheric absorption of solar radiation.

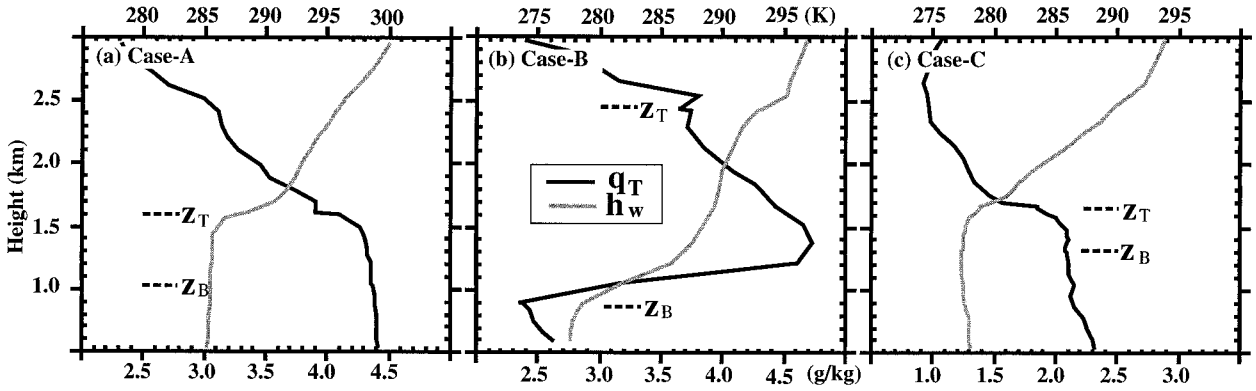

FIG. 13. As in Fig. 5 except for the mixing ratio of total water (q_T: water vapor plus liquid water) and liquid water static energy (h_w: represented by temperature): (a) case A, (b) case B, and (c) case C.

4. Results

a. Retrieved microphysical properties and comparisons with observations

Figure 12 compares the retrieved and measured vertical structures of liquid water contents and effective radii of liquid water for case A. As shown in Fig. 10, both type I and type II weighting functions are possible solutions for case A since its adiabatic cloud depth ratio (1.2) is less than the threshold value. In spite of the finer structure of the observed LWC distribution near 1.25 km, the retrieved LWC profile using a type I weighting function with $\alpha = 1.375$ appears to agree best with the observed LWC profiles from the King and FSSP probes. In regard to this finer in-cloud structure, which might be caused by the collection process of cloud water by drizzle, the type I weighting function is, however, incapable of representing this mechanism. Further, the millimeter-wavelength cloud radar was not in operation so cloud radar reflectivity data were unavailable to confirm whether this structure was real or a consequence of spatial sampling limitations of the aircraft observations.

As discussed earlier, the type I weighting function is the result of cloud-top entrainment mixing, where the subadiabatic character of in-cloud LWC depends on the entertainment rate of the dry air above the cloud-top inversion layer and its thermodynamical state (Deardorff 1980; Albrecht et al. 1985). In case A, the retrieved adiabatic LWC ratio near the cloud top is 0.28, which is close to the values found in many stratiform clouds over islands and oceans (e.g., Albrecht et al. 1985; Nicholls and Leighton 1986; Ishizaka et al. 1995). Without considering the subadiabatic character of stratiform clouds, the HW scheme can significantly overestimate the retrieved maximum LWC by about 67% for case A. This difference can be even greater in the cases that have larger adiabatic cloud depth ratios, such as the one in case B.

With the given maximum droplet number concentration from the observations ($N_0 \sim 500$ cm^{-3} in case A) and the retrieved LWC profiles (i.e., type I, type II, and adiabatic), r_e profiles can be determined from the water mass conservation equation. Note that due to the different retrieved cloud depths, the resulting N distribution used for the adiabatic LWC profile differs from its counterpart corresponding to type I and type II LWC profiles. Results indicate that all the retrieved r_e profiles show a similar shape to that of the observed distribution, which exhibits a maximum r_e near the cloud top although the pattern of the retrieved type I LWC profile substantially differs from the type II and adiabatic LWC distributions (Figs. 12a,b). Based on the r_e equation, it is not surprising that both type II and adiabatic LWC distributions yield similar r_e profiles since their maximum LWCs are located near the cloud top. In contrast, a similar retrieved r_e profile derived from the type I LWC distribution is due to the consequence that the specified N distribution near the cloud top decreases faster than the LWC profile. Among all the retrieved r_e distributions, the type I profile agrees best with the observed maximum r_e. Similar to the LWC estimation, the HW scheme can overestimate the retrieved maximum r_e by about 43% if the subadiabatic character of stratiform clouds is not considered.

Vertical profiles of the mixing ratio of total water (water vapor plus liquid) and liquid water static energy for case A are shown in Fig. 13a. Both variables remain nearly constant below 1.4 km, but change substantially aloft with height below the cloud top. This retrieved stratus cloud is nearly adiabatic two-thirds of the way up from the cloud base, but the subadiabatic character associated with cloud-top entrainment mixing becomes apparent in the remaining one-third of the cloud deck with the minimum adiabatic LWC ratio occurring near the cloud top. The thermodynamical structure of this continental stratus resembles its counterpart observed in marine stratus-topped, well-mixed boundary layers, where both type I and type II LWC profiles can exist (Albrecht et al. 1985, 1995).

In contrast to case A having a stratus-topped well-mixed boundary layer, case B exhibits decoupled cloud

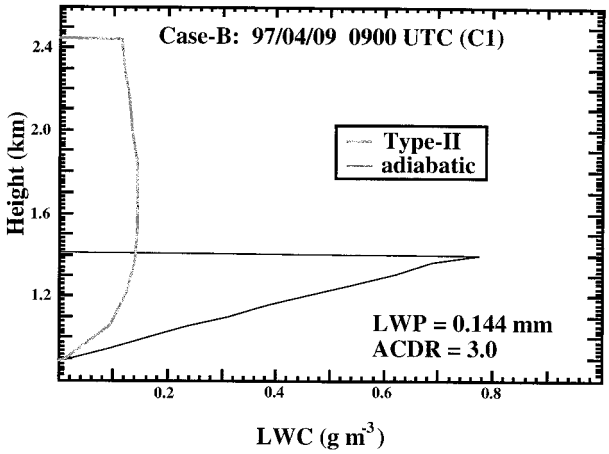

FIG. 14. Vertical profiles of retrieved LWCs for case B.

and subcloud layers (Fig. 13b). The rapid decrease of total water mixing ratio with height above 1.35 km in case B is an indication of the strong subadiabatic character. As discussed in Fig. 10, the large adiabatic cloud depth ratio of case B (ACDR = 3.0) allows only one solution to exist (i.e., type II weighting function with $\alpha = 2.91$). This solution leads to a rather uniform distribution of LWCs throughout most of the cloud deck, except for a thin layer near the cloud base (Fig. 14). A similar LWC distribution with substantial subadiabatic character was also observed in a marine stratiform cloud (Nicholls and Leighton 1986). Without considering this subadiabatic character, the HW scheme can overestimate the retrieved maximum LWC by a factor of 4.2 for this large adiabatic cloud depth ratio case.

As mentioned earlier, there are no in situ measurements available to validate the retrieved LWC profile in case B, but cloud radar reflectivity data can provide supplemental evidence for this purpose. The cloud-top height (above ground level) inferred from the MMCR at 0900 UTC 9 April 1997 is consistent with the one shown in the retrieved LWC profile (height in mean sea level) using the radiosonde data (Figs. 14 and 15a). A recent study indicates that the radar reflectivities of cloud and drizzle fields have very little overlap and are well separated by a threshold intensity around -15 dBZ (Frisch et al. 1995). Therefore, the maximum radar reflectivity of case B at 0900 UTC (about 13 dBZ) indicates the existence of drizzle in this stratus cloud, and strongly supports the retrieved type II LWC profile (Fig. 15a).

Due to the synoptic condition involved, it is believed that this decoupling was mainly caused by a low-level surge of cold and dry air outbreak associated with a southward-moving high pressure system from Canada (see Figs. 6 and 8). The intrusion of this low-level cold and dry air to the SGP site started at 0200 UTC or so. As a result, the moisture supply from the low levels to the cloud formation was cut off, leading eventually to the demise of the cloud layer due to its decoupling with the subcloud layer. The resulting temperature contrast between the warming above the inversion layer and the cooling in the subcloud layer due to the cold air surge provides an additional mechanism to stabilize the cloud layer. Similar phenomena have been reported in some marine stratus and stratocumulus cases (Nicholls 1984).

The temporal scale of synoptic-scale forcing seems not to support the initial formation of case B stratus by the frontal lifting. The warmer and moister surface air at the central facility of the SGP site ahead of the cold and dry air surge shown in Fig. 8 suggests that case B might have a well-mixed boundary layer at the initial stage around 0200 UTC or so. The coarser temporal resolution of radiosonde data is, however, unable to confirm the cause of the initial formation of stratus in this case.

To accommodate the limited in situ measurements of case C (see Fig. 4), the radiosonde data at 1800 UTC and 2100 UTC 12 April 1997 are interpolated to 1900 UTC and then combined with the data from remote sensors to retrieve the microphysical properties of the existing stratus. Similar to case A, a stratus-topped well-mixed boundary layer also existed in case C. However, this boundary layer is in a colder, drier regime so that the moisture supply for the cloud formation is less than its counterpart in case A (Figs. 5 and 7). As a result, the microwave radiometer in case C shows a very small LWP of 0.047 mm, while this magnitude is above the detectable limit.

As explained in section 2, a simple time average of the airborne data of case C provides a misleading picture on the vertical structure of the measured LWC profiles. Therefore, only two ascending subsegments of the in situ measured LWC profiles near 1900 UTC (in 1-s intervals) are used for comparison with the retrieved profiles (Fig. 16). Results indicate that the retrieved cloud depth differs substantially from the in situ measured depth, mainly due to the difference in cloud-base heights. Nonetheless, millimeter-wavelength cloud radar and ceilometer data at 1900 UTC show consistent information of the cloud geometry (i.e. cloud top and cloud base, respectively) with the retrieved cloud properties (Figs. 15b and 16); this suggests that the stratus in case C might have prominent horizontal inhomogeneity around the central facility of the SGP site.

As in case A, the small adiabatic cloud depth ratio of case C (ACDR = 1.14) allows both type I and type II weighting functions to exist in the retrieved LWC profiles. The retrieved type II LWC profile ($\alpha = 0.313$), however, appears to be in better agreement with the measured distribution near the upper portion of the cloud deck, as does the retrieved maximum LWC. The existence of light drizzle in this case is again supported by millimeter-wavelength cloud radar data, which show a maximum radar reflectivity of -12 dBZ at 1900 UTC (Fig. 15b). The application to case C is beyond the limit of a more sophisticated microphysical retrieval scheme

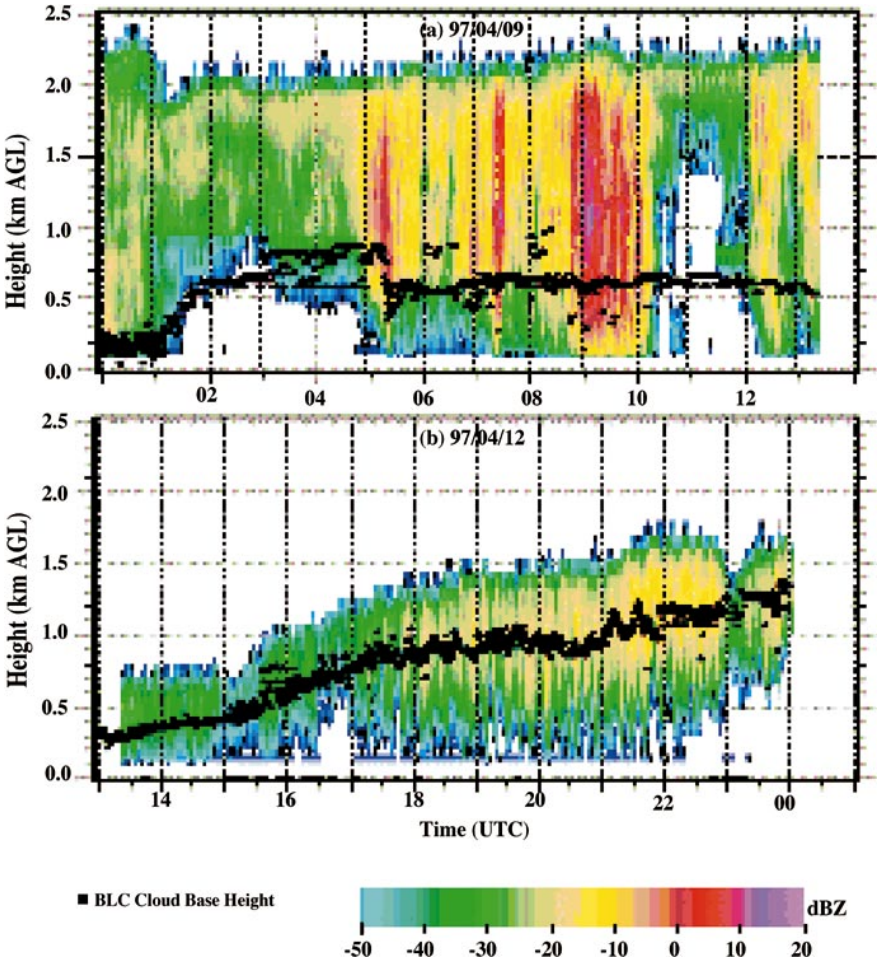

FIG. 15. Vertical profiles of MMCR reflectivity. Heights are shown in terms of above ground levels (AGL). Asterisks masks the cloud-base height given by the Belfert laser ceilometer: (a) case B, (b) case C.

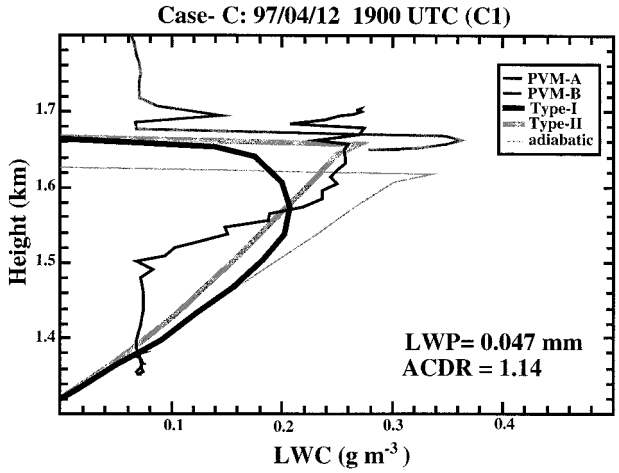

FIG. 16. As in Fig. 12a except for case C. Flight times for PVM-A and PVM-B are shown in Fig. 4.

(Frisch et al. 1995), in which the accuracy of retrieved microphysical properties seriously degrades as LWP is less than 0.1 mm or when drizzle exists. As compared to case A, the application of the HW scheme to case C leads to weaker overestimation of the retrieved maximum LWC (22% vs 67%) in this smaller adiabatic cloud depth ratio case (ACDR = 1.14 vs 1.2).

b. Impact of retrieved microphysical structures on radiation transfer

In this section, the impact of the departure of a liquid water profile from its adiabatic value on the radiative transfer is evaluated. Vertical resolution of radiation calculations within the cloud is the same as that of the retrieved microphysical properties, which have a grid spacing of 10 m at the vertical boundaries and a constant resolution of 58 m throughout the rest of the cloud deck. The spirit of this assessment is to demonstrate that simply assuming an adiabatic LWC profile and computing the cloud properties on this basis can result in significant

TABLE 2. Design of experiments for the radiation calculations of set 1. The mean LWC is based on the running mean of LWCs in the cloud deck, weighted by the in-cloud grid resolutions, and mean r_e is derived from the water mass conservation equation under the given mean LWC and droplet number concentration.

Exp	LWC profile	r_e profile	Remarks
a	Type I	Type I	
b	Type II	Type II	
aq+	Type I + 0.1	Type I	Increase LWC by 0.1 g m^{-3} every cloudy layer
ar+	Type I	Type I + 1.0	Increase r_e by 1 μm every cloudy layer
aq_m	Mean of type I	Type I	Use mean LWC (0.305 g m^{-3}) in every cloudy layer
ar_m	Type I	Mean of type I	Use mean r_e (6.05 μm) in every cloudy layer
aq_mr_m	Mean of type I	Mean of type I	Use mean LWC and r_e in every cloudy layer

radiative transfer discrepancies if the profile is actually subadiabatic. For this exercise, the radiation calculations are based solely on retrieved microphysical properties (LWC and r_e) of case A due to the availability of comprehensive in situ measurements.

Two sets of sensitivity experiments (set 1 and set 2) are performed to gauge the impacts of microphysical structures and subadiabatic characters of low-level stratiform clouds on radiative energy budgets. These impacts includes SW cloud albedo (based on Liou 1992), LW and SW cloud radiative forcings (defined as $F^{\uparrow}_{\text{clear}} - F^{\uparrow}_{\text{cloudy}}$, where $F^{\uparrow}$ is the upward flux at the top of the atmospheric column), net surface upward LW and downward SW fluxes, and radiative heating and cooling rates near the cloud boundaries. Details of the experimental design for these sensitivity experiments are shown in Tables 2 and 3. The experiments of set 1 focus on the sensitivity of radiative transfer to the types of retrieved microphysical structures, and the other set of experiments (set 2) address the radiative repercussions in various limiting circumstances, such as those in large and small adiabatic cloud depth ratios.

As discussed earlier, in situ measurements of case A support the type I retrieved LWC and r_e profiles (see Fig. 12). The subadiabatic character of this stratus cloud, which has a small adiabatic cloud depth ratio of 1.2, leads to a stronger shortwave cloud radiative forcing (SWCRF) and a weaker net surface downward SW flux than their adiabatic counterparts by 9.0 W m^{-2} and 5.3 W m^{-2}, respectively (see expt a in Table 4). Based on a global annual mean coverage of low-level stratiform clouds of 25% (Hartmann et al. 1992) and a half-day mean of the zenith angle of 60°, our calculations indicate that the difference between the estimated global-mean SWCRFs of case A and its adiabatic counterpart can be as large as -1.13 W m^{-2}. This magnitude is even larger than the direct effect of anthropogenic sulfate aerosols on global climate (-0.2 to -0.9 W m^{-2}), estimated by Chuang et al. (1997).

TABLE 3. As in Table 2 except for the experiments of set 2.

Exp	LWC profile	r_e profile	Depth ratio
a_1.15	Type I	Type I	1.15
a_1.25	Type I	Type I	1.25
b_1.15	Type II	Type II	1.15
b_1.25	Type II	Type II	1.25
b_1.5	Type II	Type II	1.5
b_2.0	Type II	Type II	2.0
b_2.5	Type II	Type II	2.5
b_3.0	Type II	Type II	3.0

The smaller effective radius of liquid water in the type I profile also leads to a stronger cloud albedo than its adiabatic counterpart by 1.3% (67.4% vs 66.1%) as a result of larger cross-sectional area for single scattering. However, the reduced r_e in the type I profile results in weaker cloud absorption than the adiabatic one by 0.6% (22.5% vs 23.1%). As a result, the net surface downward SW flux is weaker in experiment a than in the adiabatic counterpart. This r_e impact on cloud albedo and absorption is consistent with earlier studies of water clouds with LWPs greater than 0.05 mm (Stephens 1978; Liou and Wittman 1979; Slingo 1989).

In contrast, the impact of r_e profiles on longwave cloud radiative forcing (LWCRF) and net surface upward LW flux is much smaller than their SW counterparts. This result is due to the fact that water cloud acts nearly as a blackbody when the LWP is greater than 0.05 mm (Stephens 1984). Also, the subadiabatic character of stratus clouds affects its stability through radiative cooling and heating near the cloud top and cloud base, respectively. As compared to the adiabatic condition, the weaker cooling/heating rate contrast ($\Delta\dot{H}$) of 2.96 K h^{-1} in the retrieved type I microphysical structure is in response to the dominant weakening of LW cooling near the cloud top. As a result, the retrieved cloud structure with the adiabatic assumption can overestimate the destabilizing effect of the radiative process in low-level stratiform clouds.

Along with the daily mean consideration, the SW cloud radiative forcing of experiment a is -159.1 W m^{-2}, which is much stronger than the its LW counterpart (23.0 W m^{-2}). This small LWCRF is due to the low altitude of stratiform clouds in trapping less outgoing LW radiation. Although both SW and LW forcings of low-level stratiform clouds are much weaker than those of upper-level optically thick cirrus anvils (e.g., Wong et al. 1993; Chin 1994; Chin et al. 1995), these low-level clouds can have a stronger net cooling effect on the earth–atmosphere system due to the canceling effect of two comparably large cloud radiative forcings of up-

TABLE 4. Longwave and shortwave cloud radiative forcing (W m^{-2}), SW cloud albedo (α_SWcld; %), and net surface upward LW and downward SW fluxes ($F^{\uparrow}_{LW\_sfc}$ and $F^{\downarrow}_{SW\_sfc}$ in W m^{-2}) for the experiments of set 1. Results are calculated using a surface albedo of 0.2 and a zenith angle of 60°. The numbers shown are the deviations from those of the adiabatic experiment (22.5 W m^{-2}, −309.1 W m^{-2}, 66.1%, 27.0 W m^{-2}, and 73.6 W m^{-2}, respectively). The temperature change rates (K h^{-1}) of maximum SW heating and LW cooling at the cloud top ($\dot{H}_{SW\_Zt}$ and $\dot{H}_{LW\_Zt}$), LW heating at the cloud base ($\dot{H}_{LW\_Zb}$), and cooling/heating rate contrast between the cloud top and the cloud base ($\Delta\dot{H} = \dot{H}_{SW\_Zt} + \dot{H}_{LW\_Zt} - \dot{H}_{LW\_Zb}$) are deviations from those of the adiabatic experiment (2.01 K h^{-1}, −10.23 K h^{-1}, 0.7 K h^{-1}, and −8.92 K h^{-1}, respectively).

Exp	LWCRF	SWCRF	α_SWcld	$F^{\uparrow}_{LW\_sfc}$	$F^{\downarrow}_{SW\_sfc}$	$\dot{H}_{SW\_Zt}$	$\dot{H}_{LW\_Zt}$	$\dot{H}_{LW\_Zb}$	$\Delta\dot{H}$
a	0.5	−9.0	1.3	0	−5.3	−1.07	4.03	0	2.96
b	−0.2	−5.1	0.8	0.1	−3.4	−0.33	1.08	−0.05	0.80
aq+	0.5	−21.8	2.8	−0.5	−21.0	−0.79	2.5	0.24	1.47
ar+	−0.6	0.5	−0.1	0.2	3.6	−1.09	4.23	−0.01	3.15
aq_m	0.5	−9.3	1.4	−0.8	−5.8	−0.87	2.88	0.82	1.19
ar_m	0.7	−21.4	3.2	0.2	−15.0	−0.94	2.94	0	2.00
aq_mr_m	0.7	−18.8	2.8	−0.7	−12.2	−0.73	1.75	0.87	0.15

per-level anvils. Therefore, low-level stratiform clouds play an important role in the planetary radiation balance.

Similar to the adiabatic microphysical structure with larger r_e near the cloud top, experiment b with the type II retrieved profiles exhibits weaker SWCRF and cloud albedo (by 3.9 W m^{-2} and 0.5%, respectively), and stronger in-cloud cooling/heating rate contrast (by 2.16 K hr^{-1}) than those in experiment a (Table 4). The SWCRF difference of −3.9 W m^{-2} between type I and type II retrieved microphysical structures in Table 4 is equivalent to −0.49 W m^{-2} in the global annual-mean estimation, which falls in the middle range of the direct effect of anthropogenic sulfate aerosols, given by Chuang et al. (1997). Results of experiment b suggest that correct retrievals of cloud microphysical properties are still an important consideration in SW radiation budgets of global climate and in-cloud longevity.

As the LWP of cloud changes in experiment aq+ the increasing LWP substantially enhances SW fluxes and albedo. This LWP impact also acts to further destabilize the in-cloud stratification. In contrast, the larger r_e in experiment ar+ reduces the cloud albedo and its resulting SW fluxes as shown in Slingo (1989), but this impact has little effect on in-cloud radiative heating/cooling contrast.

The last three experiments of set 1 (expt aq_m, expt ar_m, and expt aq_mr_m) are designed to assess the impact of constant in-cloud LWC and r_e profiles, which are widely used in numerical models with coarser vertical grid resolution. As compared to experiment a, results indicate that the use of constant in-cloud LWC and/or r_e profiles leads to stronger SW fluxes, cloud radiative forcing, and cloud albedo than those with more detailed microphysical structures. However, these impacts are predominated by constant in-cloud r_e (see Table 4). In addition, both mean LWC and mean r_e profiles act to enhance SW heating and LW cooling effects near the cloud top, while the LW heating effect near the cloud base is mainly caused by the mean LWC profile. As a result, the use of constant in-cloud LWC and/or r_e profiles appears to strengthen the radiative in-cloud heating contrast as compared to that of experiment a.

As discussed in section 3, the type I LWC profile only exists for ACDR < 1.25, while its counterpart in type II can exist in all ACDRs. For the adiabatic cloud depth ratio of 3, the adiabatic LWC ratio of type II near the cloud top can be less than 0.1, which is rarely observed. Therefore, this value of ACDR can be viewed as the upper limit of low-level stratiform clouds. Figure 17 shows the upper limits of the subadiabatic impact of stratus cloud in case A on SW cloud albedo, and SW and LW fluxes in terms of their deviations from their adiabatic values for each type of retrieved microphysical structures. Both type I and type II microphysical structures show a consistent pattern of SW albedo and flux changes with the adiabatic cloud depth ratio (Fig. 17a); both SWCRF and SW albedo are enhanced with the increasing adiabatic cloud depth ratio mainly because of the resulting change in r_e as shown in Fig. 10. As in experiment a of set 1, the resulting smaller r_e in the experiments of set 2 weakens the cloud absorption as the adiabatic cloud depth ratio increases, but this impact is weaker than its albedo counterpart. Therefore, net surface SW flux decreases as the adiabatic cloud depth ratio becomes large. Results also indicate that for the same adiabatic cloud depth ratio, the subadiabatic impacts of the type I microphysical structures on SW albedo and SW fluxes are stronger than their type II counterparts. The upper limits of the subadiabatic impacts of these retrieved microphysical properties on SW albedo and SWCRF are 5.3% and −36.3 W m^{-2}, respectively. With the global annual-mean estimation, this upper limit of SWCRF change (−4.54 W m^{-2}) is comparable to the greenhouse warming effect (4 W m^{-2}) in the double CO_2 scenario (Manabe and Stouffer 1980; Washington and Meehl 1984).

As mentioned earlier, water clouds with the LWP greater 0.05 mm behave as blackbodies so that the subadiabatic impact of low-level clouds on LW fluxes are generally much less than their SW counterparts for all adiabatic cloud depth ratios (Fig. 17b). Besides, this LW flux impact is stronger on LWCRF than on the net surface flux due to the fact that the effective cloud-base height changes little with the adiabatic cloud depth ratio,

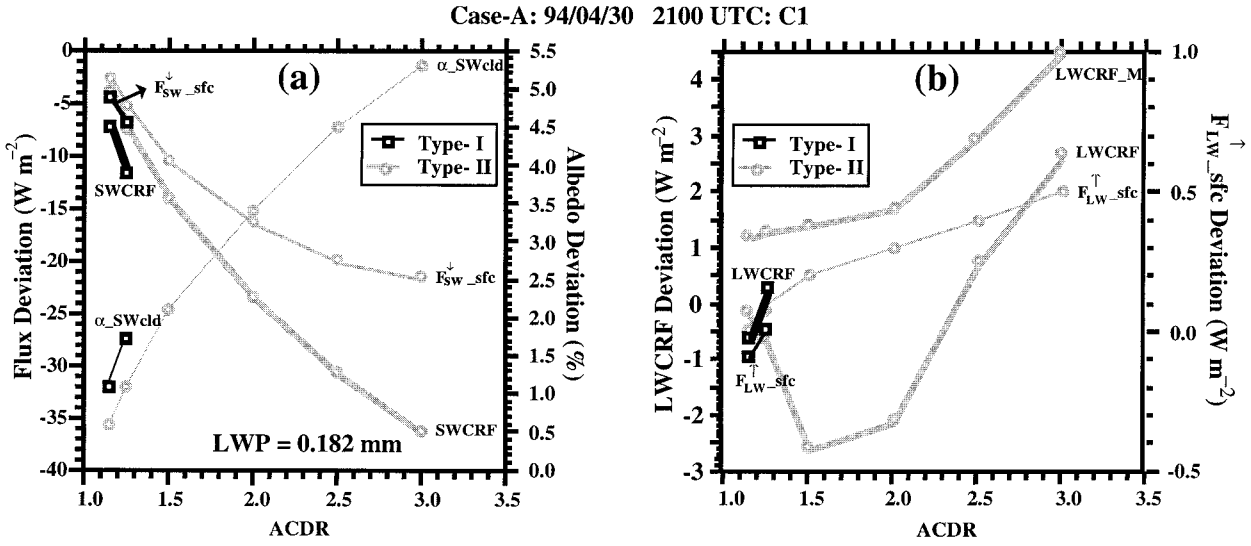

FIG. 17. Deviations of (a) SW fluxes and SW cloud albedo and (b) LW fluxes from adiabatic values, as defined in Table 4 at varied ACDRs for the experiments of set 2. LWCRF_M is the calculated LW cloud radiative forcing using the modified temperature profile as shown in Fig. 5a.

but the cloud top varies substantially. It is worth pointing out that unlike LW net surface fluxes, the resulting type II LWCRF variation exhibits an inconsistent change with the cloud structures. Further sensitivity tests indicate that this inconsistent LWCRF variation is caused by a temperature inversion above the cloud top (see Fig. 5a) since this inversion structure remains unchanged in the experiments of set 2 as the retrieved cloud structures vary with the adiabatic cloud depth ratio. Without this inversion structure, the calculated type II LW cloud radiative forcing, labeled LWCRF_M in Fig. 17b, is persistently enhanced as the adiabatic cloud depth ratio increases.

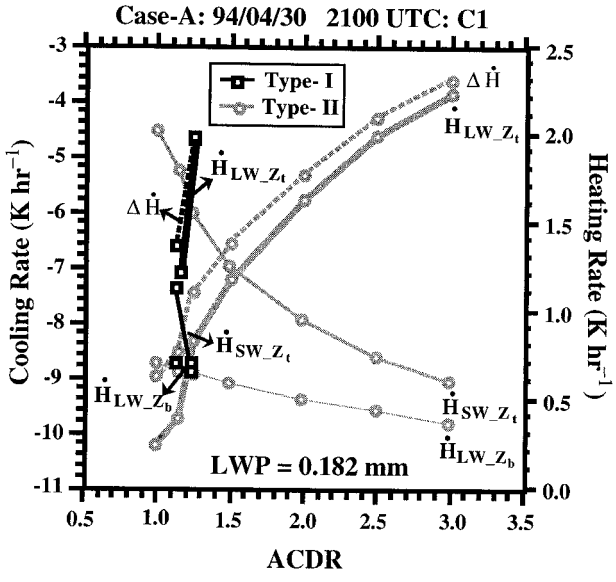

FIG. 18. The temperature change rates of maximum SW heating and LW cooling at the cloud top ($\dot{H}_{SW\_Zt}$ and $\dot{H}_{LW\_Zt}$), LW heating at the cloud base ($\dot{H}_{LW\_Zb}$), and cooling/heating rate contrast between the cloud top and the base ($\Delta\dot{H}$) at varied ACDRs for the experiments of set 2.

The variations of SW heating and LW cooling rates at the cloud top ($\dot{H}_{SW\_Zt}$ and $\dot{H}_{LW\_Zt}$, respectively), LW heating rate at the cloud base ($\dot{H}_{LW\_Zb}$), and the in-cloud cooling/heating rate contrast ($\Delta\dot{H}$) with the adiabatic cloud depth ratio are shown in Fig. 18. Both radiative heating and cooling effects near the cloud top and cloud bottom decrease with the increasing adiabatic cloud depth ratio for type I and type II microphysical structures. Therefore, the resulting in-cloud cooling/heating contrast shows similar variation with the adiabatic cloud depth ratio. This suggests that the subadiabatic character of low-level stratiform clouds acts to stabilize the cloud deck and that this impact strengthens, as the subadiabatic character becomes stronger.

5. Summary and discussion

In this paper, we demonstrate a cloud retrieval technique without using microwave radar measurements as the requirement to retrieve the internal cloud structure. This technique is developed by adding cloud-top height information into the HW scheme to provide a more realistic portrayal of the retrieved liquid water for low-level stratiform clouds with substantial adiabatic character. As a result, the modified HW scheme eliminates the need to invoke the adiabatic assumption on the retrieved LWC profiles.

Using measurements from the DOE's ARM program at the central facility of the SGP site, we evaluate this modified ground-based remote sensing technique and use it to study the impacts of the subadiabatic character

of low-level stratiform clouds on the cloud microphysical properties and radiative energy budgets. Airborne measurements and millimeter-wavelength cloud radar data are also used to validate retrieved microphysical properties. Results show that observed and retrieved microphysical properties are in fairly good agreement in both weak and strong subadiabatic conditions.

Based on the availability of airborne measurements in the ARM intensive observation periods, three stratus cloud systems occurring on 30 April 1994 (case A), 9 April 1997 (case B), and 12 April 1997 (case C) are selected in this study. These cloud systems developed under different boundary layer conditions, but all of them were accompanied by a cloud-top inversion layer. The liquid water path (LWP = 0.182, 0.144, and 0.047 mm for case A, B, and C, respectively) and the subadiabatic character (ACDR = 1.2, 3.0, and 1.14, respectively) of these clouds differ from case to case.

In this study, the modified cloud retrieval algorithm is represented by the product of a weighting function and an adiabatic LWC profile. Based on in situ measurements, two types of weighting functions are considered in this study: one is associated with a subadiabatic condition involving cloud-top entrainment mixing alone (type I) and the other accounts for both cloud-top entrainment mixing and drizzle effect (type II). While both types of weighting functions have very different vertical structures, they can be expressed in the same form given by $f(\hat{z}) = \exp(-\alpha \cdot \hat{z}^{\beta})$. Our calculations indicate that the general character of the weighting function is primarily determined by the parameter β ($\beta > 1$ for type I and $\beta < 1$ for type II). As a result of the insensitivity of β to each type of retrieved LWC profiles, β is treated as a constant in this study ($\beta = 4$ for type I and $\beta = 0.5$ for type II). Thus, the given type of weighting function is uniquely determined by the corresponding α via an iteration process under the given cloud geometry (i.e., cloud-base and cloud-top height) and integrated LWC.

Our results show that the adiabatic cloud depth ratio is a useful parameter for classifying the subadiabatic character of low-level stratiform clouds. The type I LWC profile only exists in lower adiabatic cloud depth ratio conditions, while the type II LWC profile can appear for any adiabatic cloud depth ratio. As a result, this cloud retrieval algorithm appears to be ill-posed in the low adiabatic cloud depth ratio regime. Therefore, there is no unique solution in this circumstance unless additional information, such as the presence of drizzle, is available. This information can be given from airborne measurements or millimeter-wavelength cloud radar to finalize the more appropriate solution in the low adiabatic cloud depth ratio regime.

As in the HW scheme, the usefulness of this modified cloud retrieval algorithm is still limited to single-layer clouds. Although this limitation is fairly justified in this study, further study on the statistics of single-layer structures in low-level stratiform clouds is needed to assess the performance of this retrieval algorithm to wider applications. Another limitation of the HW scheme on the temperature range of clouds warmer than -20°C might be influenced in this modified retrieval algorithm due to the addition of radiosonde data in determining the cloud-top height in this study. This problem might arise when the temperature inversion above the cloud top is not evident and/or the humidity sensor does not work properly due to the existence of ice clouds. However, the cloud-top height information from other sources enables this modified retrieval algorithm to be used in a variety of circumstances.

Results also indicate that the subadiabatic character of low-level stratiform clouds has substantial impacts on cloud heating/cooling rates and radiative energy budgets (particularly in shortwave) via the retrieved LWC distribution and its related effective radius (r_e) profile of liquid water. With the global annual-mean estimation, the adiabatic assumption of these clouds in the low adiabatic cloud depth ratio regime (ACDR < 1.25) can underestimate the shortwave cloud radiative forcing by a magnitude greater than the direct effect of anthropogenic sulfate aerosols on climate shown by Chuang et al. (1997). For an extreme case (ACDR = 3.0), this difference can be as large as the greenhouse warming effect in the double CO_2 scenario; however, this estimated SWCRF change should be viewed with caution since the global mean of low-level stratiform clouds cannot have such a large adiabatic cloud depth ratio. In addition, the impact caused by different types of retrieved microphysical properties in the low adiabatic cloud depth ratio regime is still important in SW radiation budgets and in-cloud longevity. Results further show that this subadiabatic character can act to stabilize the cloud deck by reducing the in-cloud radiative heating/cooling contrast. As a whole, these impacts strengthen as the subadiabatic character of low-level stratiform clouds increases. Therefore, the subadiabatic character of low-level stratiform clouds and their related microphysical structures are important in studying radiative energy budgets and cloud longevity.

Results further suggest that for numerical models with coarser vertical resolution, such as GCMs, the calibration of in-cloud constant r_e treatment should be taken into account in the radiative transfer parameterization as a result of its substantial influence on overestimating SW cloud albedo and SWCRF. Based on the water mass conservation, the effective radius of liquid water is dependent upon LWC and the number concentration of liquid water. Even for numerical models that have fine vertical resolutions to predict the detailed structure of LWC profiles, the parameterization of r_e to appropriately represent the subadiabatic impact of low-level stratiform clouds is impaired by the great spatial variation of N, particularly between oceans and continents, and the impact from anthropogenic pollution (e.g., Twomey et al. 1984; Leaitch et al. 1992). Therefore, the success of parameterizing r_e largely relies on the better represen-

tation of N. Although progress toward this effort has been made (e.g., Martin et al. 1994), the generality of the relationship between r_e and N in low-level strafiform clouds requires more research effort.

Acknowledgments. The authors wish to thank Drs. Y. Han and E. R. Westwater for providing us the source code of the HW scheme along with the radiosonde ensemble for use at the central facility of the ARM SGP site, and Dr. E. Clothiaux for MMCR data. This work was supported by the ARM program of the U.S. DOE, Office of Energy Research, Office of Health and Environmental Research, Environmental Sciences Division, and conducted under the auspices of the DOE by the Lawrence Livermore National Laboratory under Contract W-7405-Eng-48.

REFERENCES

Albrecht, B. A., R. P. Penc, and W. H. Schubert, 1985: An observational study of cloud-topped mixed layer. *J. Atmos. Sci.,* **42,** 800–822.

——, C. W. Fairall, D. W. Thomson, and A. B. White, 1990: Surface-based remote sensing of the observed and the adiabatic liquid water content of stratocumulus clouds. *Geophys. Res. Lett.,* **17,** 89–92.

——, S. Bretherton, D. Johnson, W. H. Schubert, and A. S. Frisch, 1995: The Atlantic Stratocumulus Transition Experiment—ASTEX. *Bull. Amer. Meteor. Soc.,* **76,** 889–904.

Chen, C., and W. R. Cotton, 1987: The physics of the marine stratocumulus-capped mixed layer. *J. Atmos. Sci.,* **44,** 2951–2977.

Chin, H.-N. S., 1994: The impact of the ice phase and radiation on a midlatitude squall line. *J. Atmos. Sci.,* **51,** 3320–3343.

——, Q. Fu, M. M. Bradley, and C. R. Molenkamp, 1995: Modeling of a tropical squall line in two dimensions: Sensitivity to radiation and comparison with a midlatitude case. *J. Atmos. Sci.,* **52,** 3172–3193.

Chuang, C. C., J. E. Penner, K. E. Taylor, and A. S. Grossman, 1997: An assessment of the radiative effects of anthropogenic sulfate. *J. Geophys. Res.,* **102,** 3761–3778.

Clothiaux, E. E., and Coauthors, 1999: The Atmospheric Radiation Measurement program cloud radars: Operational modes. *J. Atmos. Oceanic Technol.,* **16,** 819–827.

Cotton, W. R., 1975: On parameterization of turbulent transport in cumulus clouds. *J. Atmos. Sci.,* **32,** 548–564.

Deardorff, J. W., 1980: Cloud top entrainment instability. *J. Atmos. Sci.,* **37,** 131–147.

Dong, X., T. P. Ackerman, E. E. Clothiaux, P. Pilewskie, and Y. Han, 1997: Microphysical and radiative properties of boundary stratiform clouds deduced from ground-based measurements. *J. Geophys. Res.,* **102,** 23 829–23 843.

Frisch, A. S., C. W. Fairall, and J. B. Snider, 1995: Measurements of stratus cloud and drizzle parameters in ASTEX with a K_α-band Doppler radar and a microwave radiometer. *J. Atmos. Sci.,* **52,** 2788–2799.

Fu, Q., and K.-N. Liou, 1993: Parameterization of the radiative properties of cirrus clouds. *J. Atmos. Sci.,* **50,** 2008–2025.

——, ——, M. C. Cribb, T. P. Charlock, and A. Grossman, 1997: On multiple scattering parameterization in thermal infrared radiation transfer. *J. Atmos. Sci.,* **54,** 2799–2812.

——, M. C. Cribb, H. W. Barker, S. K. Krueger, and A. Grossman, 2000: Cloud geometry effects on atmospheric solar absorption. *J. Atmos. Sci.,* **57,** 1153–1168.

Han, Y., and E. R. Westwater, 1995: Remote sensing of tropospheric water vapor and cloud liquid water by integrated ground-based sensors. *J. Atmos. Oceanic Technol.,* **12,** 1050–1059.

Hartmann, D. L., M. E. Ocker-Bell, and M. L. Michelsen, 1992: The effects of cloud type on earth's energy balance: Global analysis. *J. Climate,* **5,** 1281–1304.

Ishizaka, Y., Y. Kurahashi, and H. Tsuruta, 1995: Microphysical properties of winter stratiform clouds over the southwest island area in Japan. *J. Meteor. Soc. Japan,* **73,** 1137–1151.

Leaitch, W. R., G. A. Issac, J. W. Strapp, C. M., Banic, and H. A. Wiebe, 1992: The relationship between cloud droplet number concentrations and anthropogenic pollution: Observations and climatic implications. *J. Geophys. Res.,* **97,** 2463–2474.

Liao, L., and K. Sassen, 1994: Investigation of relationships between Ka-band radar reflectivity and ice and liquid water contents. *Atmos. Res.,* **34,** 231–248.

Liou, K.-N., 1992: *Radiation and Cloud Processes in the Atmosphere.* Oxford University Press, 487 pp.

——, and G. D. Wittman, 1979: Parameterization of the radiative properties of clouds. *J. Atmos. Sci.,* **36,** 1261–1273.

Manabe, S., and R. J. Stouffer, 1980: Sensitivity of a global climate model to an increase of CO_2 concentration in the atmosphere. *J. Geophys. Res.,* **85,** 5529–5554.

Martin, G. M., and D. W. Johnson, 1992: The measurements and parameterization of effective radius of droplets in stratocumulus clouds. *Proc. 11th Int. Conf. on Clouds and Precipitation,* Vol. 1, Montreal, PQ, Canada, International Commission on Clouds and Precipitation and International Association of Meteorology and Atmospheric Physics, 158–161,

——, ——, and A. Spice, 1994: The measurement and parameterization of effective radius of droplets in warm stratocumulus clouds. *J. Atmos. Sci.,* **51,** 1823–1842.

Nicholls, S., 1984: The dynamics of stratocumulus: Aircraft observations and comparisons with a mixed layer model. *Quart. J. Roy. Meteor. Soc.,* **110,** 783–820.

——, and J. Leighton, 1986: An observational study of the structure of stratiform cloud sheets: Part I. Structure. *Quart. J. Roy. Meteor. Soc.,* **112,** 431–460.

Noonkester, V. R., 1984: Droplet spectra observed in marine stratus cloud layers. *J. Atmos. Sci.,* **41,** 829–845.

Paluch, I. R., C. A. Knight, and L. J. Miller, 1996: Cloud liquid water and radar reflectivity of nonprecipitating cumulus clouds. *J. Atmos. Sci.,* **53,** 1587–1603.

Politovich, M. K., B. B. Stankov, and B. E. Martner, 1995: Determination of liquid water altitudes using combined remote sensors. *J. Appl. Meteor.,* **34,** 2060–2075.

Ramanathan, V., R. D. Cess, E. F. Harrison, P. Minnis, B. R. Barkstrom, E. Ahmad, and D. L. Hartmann, 1989: Cloud-radiative forcing and climate: Results from the Earth Radiation Budget Experiment. *Science,* **243,** 57–63.

Rogers, D. P., and J. W. Telford, 1986: Metastable tops. *Quart. J. Roy. Meteor. Soc.,* **112,** 481–500.

Slingo, A., 1989: A GCM parameterization for the shortwave radiative properties of water clouds. *J. Atmos. Sci.,* **46,** 1419–1427.

——, S. Nicholls, and J. Schmetz, 1982: Aircraft observations of marine stratus during JASIN. *Quart. J. Roy. Meteor. Soc.,* **108,** 833–856.

Stephens, G. L., 1978: Radiation profiles in extended water clouds. Part II: Parameterization schemes. *J. Atmos. Sci.,* **35,** 2123–2132.

——, 1984: The parameterization of radiation from numerical weather prediction and climate models. *Mon. Wea. Rev.,* **112,** 826–867.

Twomey, S., M. Piepgrass, and T. L. Wolfe, 1984: An assessment of the impact of pollution on global cloud albedo. *Tellus,* **36B,** 356–366.

Washington, W. M., and G. A. Meehl, 1984: Seasonal cycle experiment on the climate sensitivity due to a doubling of CO_2 with an atmospheric general circulation model coupled to a simple mixed-layer ocean model. *J. Geophys. Res.,* **89,** 9475–9503.

Westwater, E. R., 1978: The accuracy of water vapor and cloud liquid determination by dual-frequency ground-based microwave radiometry. *Radio Sci.,* **13,** 677–685.

Wong, T., G. L. Stephens, P W. Stackhouse Jr., and F. P. J. Valero, 1993: The radiative budgets of a tropical mesoscale convective system during EMEX-STEP-AMEX experiment. II: Model results. *J. Geophys. Res.,* **98,** 8695–8711.